


Article

Batch and Column Adsorption of Phosphorus by Modified Montmorillonite

Zhonghao He ^{1,†}, Jiajun Chen ^{1,2,†} , Jianzun Lu ^{1,2}, Sabrina Yanan Jiang ^{3,*}, Lingcheng Su ¹, Chiu Hong Lee ¹ and Huada Daniel Ruan ^{1,*}

¹ Environmental Science Program, Division of Science and Technology, Beijing Normal University-Hong Kong Baptist University United International College, Zhuhai 519087, China; lionelhe10@163.com (Z.H.); gzchenjiajun@163.com (J.C.); jianzunlu@uic.edu.cn (J.L.); sulingcheng@163.com (L.S.); chiuHonglee@uic.edu.cn (C.H.L.)

² Department of Chemistry, Faculty of Science, Hong Kong Baptist University, Hong Kong 999077, China

³ National Observation and Research Station of Coastal Ecological Environments in Macao, Macao Environmental Research Institute, Macau University of Science and Technology, Taipa 999078, Macao, China

* Correspondence: ynjiang@must.edu.mo (S.Y.J.); hruan@uic.edu.cn (H.D.R.)

† These authors contributed equally to this work.

Abstract: Phosphorus pollutants are a crucial component of water eutrophication. In this study, montmorillonite modified by Keggin Al_{13} and hexadecyltrimethyl ammonium (Al_{13} -O-MMt) was used as an adsorbent to remove phosphorus from solutions and thus simulate the practice of a field trial, such as in wastewater. The ammonium molybdate spectrophotometric method was used to determine the concentrations of phosphorus in samples. In the batch experiment, phosphorus was adsorbed by original montmorillonite (MMt) and Al_{13} -O-MMt at various pH values (6–9) to identify the effect of pH during the adsorption process. The batch adsorption results demonstrate that Al_{13} -O-MMt can adsorb up to 93% of phosphorus at pH = 8. Six graduated amounts (0.01–0.25 g) of montmorillonite were tested at three different temperatures to determine the most suitable temperature and the minimum dosage of Al_{13} -O-MMt needed for the adsorption of 200 mg/L phosphorus in a 30 mL solution, which was 0.1 g at 25 °C. Therefore, the adsorption capacity of Al_{13} -O-MMt was found to be 60 mg/g. Subsequently, a column experiment was conducted. The results showed that the optimized dosage of Al_{13} -O-MMt was 6.667 g for phosphorus adsorption with a concentration of 200 mg/L in 2000 mL solution, and the breakthrough time was 4794.67 min.

Keywords: column adsorption; modified montmorillonite; phosphorus; batch adsorption



Citation: He, Z.; Chen, J.; Lu, J.; Jiang, S.Y.; Su, L.; Lee, C.H.; Ruan, H.D. Batch and Column Adsorption of Phosphorus by Modified Montmorillonite. *Appl. Sci.* **2022**, *12*, 5703. <https://doi.org/10.3390/app12115703>

Academic Editor: Bart Van der Bruggen

Received: 6 May 2022

Accepted: 30 May 2022

Published: 3 June 2022

Publisher's Note: MDPI stays neutral with regard to jurisdictional claims in published maps and institutional affiliations.



Copyright: © 2022 by the authors. Licensee MDPI, Basel, Switzerland. This article is an open access article distributed under the terms and conditions of the Creative Commons Attribution (CC BY) license (<https://creativecommons.org/licenses/by/4.0/>).

1. Introduction

Montmorillonite is a soft clayey water-absorbent mineral. It is a hydrous aluminum silicate with perceivable layers and sheets, with the general formula of $(Na,Ca,K)_{x+y}(Si_{y-x}Al_x)(Al_{2-y}Mg_y) \cdot O_{10}(OH)_2$, where $x = 0.05$ – 0.45 and $y = 0.05$ – 0.65 . Each layer is composed of two types of structural sheets: octahedral and tetrahedral [1,2]. A unit of montmorillonite contains two tetrahedral layers and an octahedral layer between these two tetrahedral layers. They are turned towards each other by similarly charged oxygen layers, so as to stabilize the aluminum (magnesium)–oxygen–hydroxylayers by the van der Waals forces [3,4].

Montmorillonite possesses good adsorption and cation exchange capacity (CEC). The Si^{4+} in the tetrahedral layers can be replaced by Al^{3+} , and Al^{3+} in the octahedral layers in montmorillonite can be replaced by Zn^{2+} , Mn^{2+} , Li^+ , or Fe^{3+} to form interlayer negative charges [5]. The negative charge is balanced by potassium and sodium ions outside the layered structure. Ions, water, and salts can enter and leave the interlayer of montmorillonite under environmental conditions [6,7]. In this way, inorganic and organic montmorillonite complexes are formed. A modified adsorbent with a good adsorption effect can be prepared based on the porous property of montmorillonite after modification by anions or/and

cations through cation exchange on the surface or interlayer and intercalation of organic compounds into the interlayer. Additionally, montmorillonite has been adopted as a good adsorbent on account of the existence of different types of active sites located on its surfaces, such as ion-exchange sites, Lewis acid sites, and Bronsted sites [5,8]. The efficiency and effectiveness of the adsorbent are the key factors in adsorption techniques [9]. However, untreated montmorillonite does not effectively remove targeted pollutants during wastewater treatment processes due to the extremely strong hydrophilicity of the silica structure on its surface and the hydrolysis of interlayer cations; thus, its adsorption performance should be improved by modification [10–12].

Studies have revealed that modification has a certain effect on the adsorption capacity of montmorillonite [13–15]. Nie et al. performed an XRD analysis of C₁₂ alkyl polyglycolide quaternary ammonium-modified montmorillonite, suggesting that as the interlayer spacing increased, the number of exchangeable ions between the montmorillonite layers increased, and the specific surface area decreased compared to that of untreated montmorillonite [10]. Jang et al. reported that with an increase in hexadecyltrimethyl ammonium (HDTMA), the specific surface area of the modified montmorillonite decreased and the number of effective sites available for Cr(VI) adsorption also decreased, weakening the strength of purely physical adsorption; meanwhile, the surface electrical properties of the modified montmorillonite changed from negative to positive, reflecting that electrostatic adsorption was enhanced for anionic pollutants [16].

Notably, the pH value of the solution may affect the removal efficiency since the surface charge density of montmorillonite changes with the ionization of adsorbate species [17–21]. Wang et al. found that the impacts of pH on adsorption of U(VI) on Na-MMt and OH-Al-MMt were greatly dependent on pH, and the amount adsorbed decreased with the increase in the pH from 4.0 to 8.0 [22]. Rezala et al. showed that OH-Al-MMt adsorption indicated that the removal of methylene blue dye increased with an increase in the pH, up to a pH of 8 in solution. However, the methylene blue uptake capacity did not change from pH 8 to 10 [23]. Furthermore, temperature variation influences the adsorption rate of modified montmorillonite [24–28]. Wang et al. demonstrated that the amount of the herbicide paraquat adsorbed by montmorillonite increased with a decreasing adsorption temperature in a physical exothermic adsorption process [29]. On the contrary, Manohar et al. discovered that an increase in temperature could lead to an increase in the retention effect of metal on clay, presenting an endothermic reaction [30]. pH and temperature were two key factors used to discern the adsorption mechanism between the adsorbate and the adsorbent in the above adsorption experiments. In previous studies focusing on the adsorption abilities of modified MMt, batch adsorption has been a common method for studying the amounts of different pollutants adsorbed by modified MMt [31–33]. Batch adsorption is mostly conducted in the laboratory, making it difficult to apply in industrial wastewater treatment [34–37]. Therefore, the design of a column adsorption facility is a necessary procedure that can be applied towards actual industrial water and wastewater treatments [38–41].

It has been reported that the total phosphorus discharge in China was 0.54 million tons in 2015, according to statistics [42]. Most inlet phosphorus concentrations for wastewater treatment plants (WWTPs) in China are in the range of 5–20 mg/L [43–45]. High concentrations of phosphorus in water cause damage to the ecosystem and even to human health. Phosphorus discharge can lead to skin inflammation in humans and eutrophication in the water system [46–49]. Therefore, the adsorption of phosphorus via the increased adsorbability of modified montmorillonite has been applied as a solution to this problem [50–52].

This study aims to reveal whether modified montmorillonite has an excellent adsorption efficiency for phosphorus in batch and column adsorption experiments. The optimal conditions of phosphorus adsorption were investigated by studying the effects of pH, concentration of phosphorus, temperature, and adsorbent dosage on phosphorus adsorption efficiency. In addition, an elution column was used to conduct a column adsorption experiment to determine the breakthrough time. Furthermore, XRD analysis was

used to study the changes in the interlayer structure of the modified MMt before and after batch and column adsorptions to further confirm the enhancement of phosphorus adsorption resulting from interlayer variations in modified MMt. The results of this study may provide a new solution for the removal of phosphorus in factory sewage, as well as a waste-utilization methodology for the application of montmorillonite mineral-containing waste materials to fabricate environmentally friendly adsorbents.

2. Materials and Methods

2.1. Material and Chemicals

The montmorillonite used was purchased from the high-purity clay mineral sample library (highly pure clay mineral >95%). The AlCl_3 and Na_2CO_3 used in the modification of montmorillonite are AR grade and they were purchased from Damao Chemical (Tianjin, China) and Guangfu Technology Development Co. Ltd. (Tianjin, China), respectively. The reference code used for the XRD pattern of MMt was PDF#13-0135. Monopotassium phosphate (MKP) and ammonium chloride solution, which are AR grade, were obtained from Xilong Scientific (Foshan, China) and Damao Chemical (Tianjin, China), respectively. Potassium persulfate and sodium molybdate (Baishi Chemical, Tianjin, China) were employed to prepare the phosphorus stock solution. Ascorbic acid (AR grade) was purchased from Xilong Scientific (Foshan, China) for the purpose of detecting the concentration of phosphorus in the samples.

2.2. Preparation of Modified Montmorillonite

Firstly, the Keggin Al_{13} complex was synthesized, following the procedure reported by Ma et al., 2016 [53]. To synthesize the Keggin Al_{13} complex, 400 mL of 0.5 M Na_2CO_3 was added dropwise into 960 mL of 1.0 M AlCl_3 solution in ultrapure water at 60 °C with magnetic stirring for 12 h and aging at 60 °C for 24 h. For simultaneous adding of the modifier, 1.0 CEC (the CEC of MMt is 113 mmol/100 g, using a hexamminecobalt trichloride solution) hexadecyltrimethyl ammonium (HDTMA) was added into the Keggin Al_{13} complex solution to obtain a solution with two modifiers. Then, the modification of MMt was accomplished by adding 40 g of MMt to the modifier solution and mixing at 25 °C for 24 h, followed by an aging process at 60 °C for 24 h. Afterward, the excess modifying solvent was washed off using DI water and centrifuged at 6000 rpm to obtain a solid cake. After being dried at 80 °C for 15 h, modified MMt was obtained. The sample was ground into fine particles and passed through a 200-mesh to obtain the samples with a 0.074 mm size. The sample was named $\text{Al}_{13}\text{-O-MMt}$.

2.3. Preparation of Phosphorus Stock Solution

Using the ammonium molybdate spectrophotometric method (GB 11893-89,1989), 0.2197 g of monopotassium phosphate (KH_2PO_4) was dissolved in DI water after being dried for 2 h at 105 °C. Then, 5 mL of 50% sulfuric acid was added and the volume of the solution was increased to 1000 mL using DI water.

2.4. The Morphology of MMt and $\text{Al}_{13}\text{-O-MMt}$ as Characterized by Scanning Electron Microscope (SEM)

A ZEISS EVO18 scanning electron microscope (SEM) was used to investigate the morphologies on the surfaces of MMt and $\text{Al}_{13}\text{-O-MMt}$. Before the investigation, the samples were plated with gold to enhance their conductivity.

2.5. Batch Adsorption of Phosphorus by $\text{Al}_{13}\text{-O-MMt}$

2.5.1. Experiment Regarding the Effect of pH on Phosphorus Adsorption

In this batch adsorption experiment, both $\text{Al}_{13}\text{-O-MMt}$ and original montmorillonite (MMt) were used as adsorbents to adsorb phosphorus in solutions at different pH values to reveal the most suitable adsorbent as well as the best adsorption efficiency. Specifically, 0.3 g of $\text{Al}_{13}\text{-O-MMt}$ or MMt was weighed into a 50 mL centrifuge tube. According to the

integrated wastewater discharge standard (GB8978, 1996), phosphorus solutions at pH 6, 7, 8 and 9 were adjusted using 0.1 M hydrochloric acid or 0.1 M sodium hydroxide to simulate wastewater at different pH values. Then, 30 mL of 2 mg/L phosphorus standard solution was added into each centrifuge tube. Finally, all samples were placed in a shaker (TY-80A/S, Ronghua Ltd., Changzhou, China) at room temperature. After being shaken at 150 rpm for 24 h, the supernatant of each sample was filtered through a 0.45 μm syringe filter membrane (MCE, Jinteng, Tianjin, China) into a colorimetric tube. The concentration of phosphorus in the colorimetric tube was determined following the ammonium molybdate spectrophotometric method (GB 11893-89, 1989). The adsorption efficiency of phosphorus onto $\text{Al}_{13}\text{-O-MMt}$ was calculated by the following equation:

$$R\% = \frac{C_0 - C}{C_0} \times 100\%, \quad (1)$$

where $R\%$ is adsorption efficiency, %, and c_0 and c are the initial and equilibrium concentrations of solute in solution, mg/L, respectively.

2.5.2. Experiment Regarding the Effect of Concentration on Phosphorus Adsorption at Different Temperatures

In this experiment, eight concentration gradients of phosphorus solutions (2, 5, 10, 20, 50, 100, 150, and 200 mg/L), at 30 mL each, were added to centrifuge tubes with 0.3 g $\text{Al}_{13}\text{-O-MMt}$. The pH of each solution was adjusted to 8 to maximize the adsorption capacity as obtained from the experiment on the effect of pH. Then, the solution in the centrifuge tubes was shaken at 150 rpm on a shaker for 24 h at the three temperatures of 25, 35, and 45 $^{\circ}\text{C}$. Triplicate samples were conducted in the experiment. The adsorption efficiency was determined with the method described in Section 2.5.1.

2.5.3. Experiment Regarding the Effect of Adsorbent Dosage on Phosphorus Adsorption

Six dosage gradients of $\text{Al}_{13}\text{-O-MMt}$ with 0.01, 0.05, 0.1, 0.15, 0.2, and 0.25 g were prepared in the centrifuge tubes. Then, 30 mL of 200 mg/L phosphorus solution with pH equal to 8 (the maximum initial concentration of phosphorus with 95% adsorption efficiency, based on the results from the experiment on the effect of concentration) was added into the centrifuge tube containing $\text{Al}_{13}\text{-O-MMt}$. Then, the solution was shaken at 150 rpm on a shaker for 24 h. The adsorption efficiency was determined using the method mentioned in Section 2.5.1.

2.6. Column Adsorption Experiment in Elution Column

In the column adsorption experiment, $\text{Al}_{13}\text{-O-MMt}$ adsorbent was used to treat 2000 mL of 200 mg/L phosphorus. As the results in the experiment on the effect of adsorbent dosage on phosphorus adsorption indicate that the optimal dosage of $\text{Al}_{13}\text{-O-MMt}$ is 0.1 g for the adsorption of 30 mL of 200 mg/L phosphorus, as was demonstrated in the batch adsorption experiment, the amount of $\text{Al}_{13}\text{-O-MMt}$ used in the column experiment could be calculated as follows:

$$\text{Amount} = \frac{\text{total amount of phosphor in aqueous solution}}{\text{adsorbed amount of phosphor by per g of } \text{Al}_{13} - \text{O} - \text{MMt}}$$

$$\text{Amount} = \frac{\frac{200 \text{ mg}}{1 \text{ L}} \times \frac{1 \text{ L}}{1000 \text{ mL}} \times 2000 \text{ mL}}{\frac{\frac{200 \text{ mg}}{1 \text{ L}} \times \frac{1 \text{ L}}{1000 \text{ mL}} \times 30 \text{ mL}}{0.1 \text{ g}}} \approx 6.667 \text{ g}$$

A total amount of 6.667 g $\text{Al}_{13}\text{-O-MMt}$ was then weighed and placed in the column to treat 2000 mL of 200 mg/L phosphorus solution at pH 8. A 0.45 μm filter membrane (Jinteng, Tianjin, China) was placed at the bottom of an elution column (Huida Laboratory Consumables, Chongqing, China).

Next, 6.667 g of Al₁₃-O-MMt was packed into the empty elution column and connected to a constant flow pump (KSP-F01A, Kamoer, Shanghai, China) with a flow rate of 0.417 mL/min (Figure 1). Afterwards, 200 mL of the phosphorus solution (200 mg/L) was added and drawn evenly across an 8 h period per day. The experiment spanned 12 days (2000 mL in 10 days was obtained from the prediction in the batch experiment, 400 mL in 2 days was used for error detection), and a total of 2400 mL of 200 mg/L phosphorus solutions was loaded into the column to ensure that the adsorbent was saturated. The operation duration for each day was 8 h. Moreover, 200 mL of sample was collected each day, and 12 samples were collected at the end of Al₁₃-O-MMt adsorption after 12 days. The same method (GB 11893-89) as that used in the batch adsorption experiment was applied to determine the concentration of phosphorus in a daily sample of this column experiment.

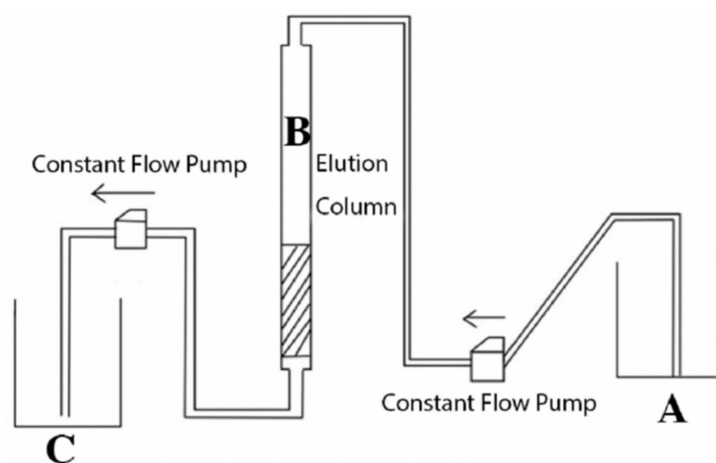


Figure 1. Column adsorption device for removal of phosphorus. **A** indicates the prepared phosphorus solution, **B** represents the elution column filled with Al₁₃-O-MMt, and **C** denotes the solution after treatment from Al₁₃-O-MMt.

2.7. Calculation of Breakthrough Time

The Thomas model is widely used to describe in-column performance, assuming that the adsorption process is managed by the mass transfer processes at the interphase species and is not limited to the chemical reaction between the substrate and adsorbent [54]. This model is expressed as:

$$\frac{c}{c_0} = \frac{1}{1 + \exp\left(\frac{k_{TH}q_0x}{v} - k_{TH}C_0t\right)} \quad (2)$$

where c_0 and c (mg/L) are the initial and equilibrium concentrations of solute in solution, respectively; q_0 denotes the adsorption capacity (mg/g); k_{TH} indicates the Thomas rate constant (mL/min·mg); x represents the quantity of montmorillonite used in the column experiment; v is the flow rate; and t designates the breakthrough time needed by the experiment [16].

2.8. Analysis for Further Confirmation of Phosphorus Adsorption

X-ray diffraction (XRD) was performed to further confirm phosphorus adsorption by analyzing the composition of Al₁₃-O-MMt before and after batch and column adsorptions. The performance of Al₁₃-O-MMt in adsorbing phosphorus could be identified through the changes between layers of Al₁₃-O-MMt in the XRD patterns.

For XRD analysis, a random powder sample was prepared by weighing about 100 mg of each sample and backfilling in a sample holder. Each sample was detected through XRD (D8 Advance, Bruker, Germany) with the Cu-target at 40 kV, 40 mA, and a step size of 0.05°. The XRD patterns were recorded at 3°–70° 2θ.

3. Results and Discussion

3.1. The Morphology of MMt and Al₁₃-O-MMt

Figure 2 shows that MMt has larger plates with a platy structure, while Al₁₃-O-MMt has smaller aggregated plates with small particles, indicating that the modifications by the Keggin Al₁₃ complex and HDTMA caused the changes in particle size and even morphology, which might have improved the ability to adsorb pollutants.

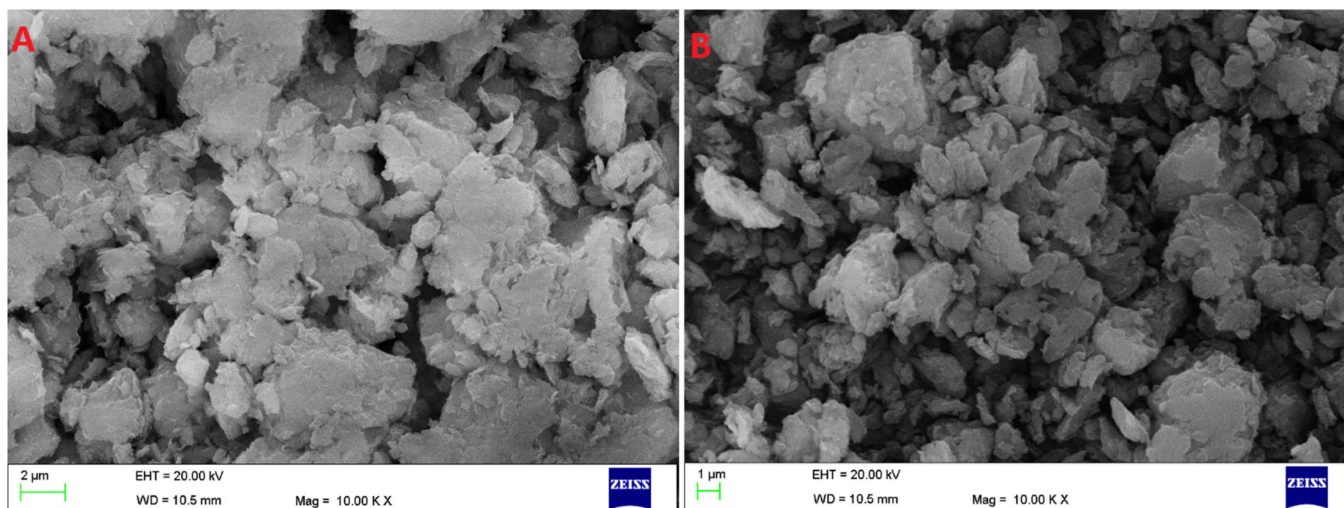


Figure 2. The morphology of MMt (A) and Al₁₃-O-MMt (B) characterized by SEM.

3.2. The Batch Adsorption of Phosphorus by Al₁₃-O-MMt

3.2.1. Effect of pH on Phosphorus Adsorption by Al₁₃-O-MMt

Figure 3 shows that the adsorption efficiency of Al₁₃-O-MMt is higher than MMt in the pH range of 6–9. Phosphate is a form of phosphorus in aqueous solution, which has a negative charge. Modifiers occupying the negatively charged sites of MMt can reduce the electrostatic repulsion between the phosphate and adsorbent, resulting in an increase in the adsorption efficiency of Al₁₃-O-MMt. In addition, the Lewis acidity sites from the Keggin Al₁₃ complex can attract substances with a negative charge [55–57]. Therefore, the adsorption efficiency of phosphorus onto Al₁₃-O-MMt is better than that onto MMt. Figure 3 indicates that the pH has an effect on the efficiency of the adsorption of phosphorus onto both Al₁₃-O-MMt and MMt. The efficiency of the adsorption of phosphorus onto Al₁₃-O-MMt increased from pH 6 to 8. This is because the concentration of OH[−] increases with the increase in pH in the range of 6 to 8, causing HPO₄[−] to transform into PO₄^{2−}, and PO₄^{2−} can be more easily adsorbed by Keggin Al₁₃ [58]. The decrease in adsorption efficiency with a further increase in pH could be explained that the increase in negative charges on the Al₁₃-O-MMt surface can result in strengthening electrostatic repulsion between adsorbent and phosphorus. In addition, the high concentration of OH[−] competes with PO₄^{2−}, contributing to a decrease in the adsorption of phosphorus [16]. For the adsorption of phosphorus onto MMt, the adsorption efficiency of phosphorus decreased with increasing pH (Figure 3). This could be explained by, similar to the explanation for the adsorption of phosphorus onto Al₁₃-O-MMt, the increasing pH changing the surface charge of MMt to make it more negative, thereby increasing the electrostatic repulsion between adsorption sites and phosphorus.

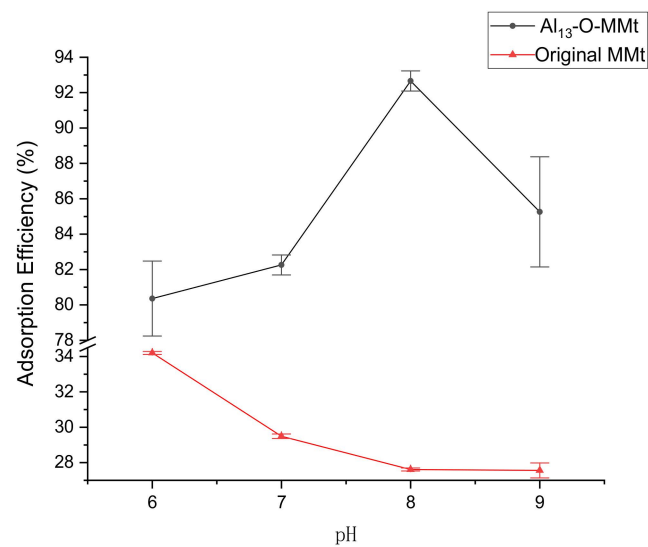


Figure 3. Adsorption efficiency (%) of MMt and Al₁₃-O-MMt for phosphorus at different pH values.

3.2.2. Effect of Initial Concentration of Phosphorus and Adsorption Temperature on Phosphorus Adsorption by Al₁₃-O-MMt

Since eight concentration gradients were used in this experiment and the amount of phosphorus adsorbed increased as the initial concentration of phosphorus increased, the increase in phosphorus ions could have led the reaction towards adsorption until all the adsorption sites were filled. An increase in phosphorus in the solution further promoted the entry of phosphorus into the interlayer of the adsorbent. Consequently, the total amount of phosphorus adsorbed increased with increasing phosphorus ions in the solution (Figure 4A). However, the adsorption efficiency decreased with the increasing initial concentration of phosphorus, as with the continuing increase in phosphorus in solution, additional phosphorus would not be able to enter the adsorption sites that were already filled [59]. In particular, the adsorption efficiency was higher than 95% at 25 °C, suggesting that the adsorption efficiency was almost stable with the increasing concentration of phosphorus at 25 °C. However, the adsorption efficiencies decreased as the concentration of phosphorus in the solution increased in the cases of 35 °C and 45 °C (Figure 4B).

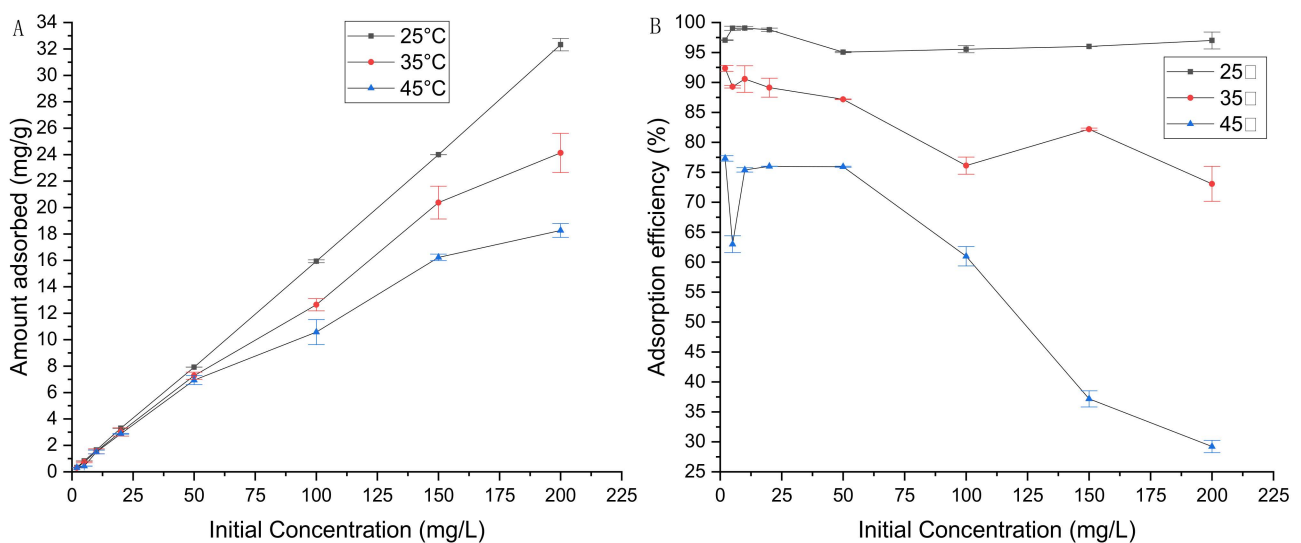


Figure 4. Three temperature gradients were measured to determine the amount adsorbed (A) and adsorption efficiency (B) of Al₁₃-O-MMt in different initial concentrations of phosphorus.

As illustrated in Figure 4, the phosphorus adsorption efficiency of $\text{Al}_{13}\text{-O-MMt}$ decreased as the temperature increased from 25 °C to 45 °C, revealing that phosphorus adsorption was spontaneously exothermic. The increasing temperature might have weakened the interrelation between phosphorus and $\text{Al}_{13}\text{-O-MMt}$ and even destroyed the active binding sites [60]. Additionally, a higher temperature would accelerate ion mobility and the desorption of phosphorus ions. Furthermore, part of the $\text{Al}_{13}\text{-O-MMt}$ might have dissolved at higher temperatures, resulting in the decrease in adsorption efficiency.

3.2.3. Effect of the Amount of $\text{Al}_{13}\text{-O-MMt}$ on Phosphorus Adsorption

Figure 5 illustrates that the adsorption efficiency of phosphorus onto $\text{Al}_{13}\text{-O-MMt}$ increased with the increase in the dosage of the adsorbent and became stable at ~95% when the dosage was 0.1 g. An increasing dosage of adsorbent could adsorb more phosphorus in the aqueous solution. When the dosage reached 0.1 g, the adsorption of phosphorus onto $\text{Al}_{13}\text{-O-MMt}$ approached the equilibrium status, in which nearly the optimal amount of phosphorus was adsorbed. For reasons of cost-effectiveness, based on the experimental data, 0.1 g adsorbent is the optimal amount for the removal of 30 mL of 200 mg/L phosphorus.

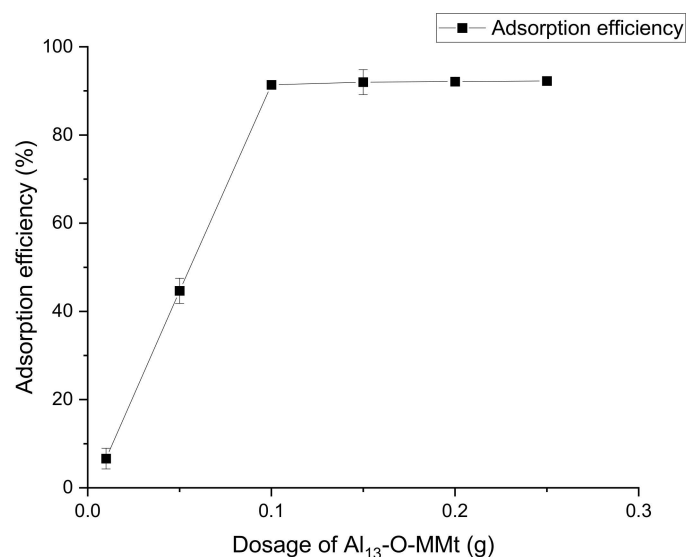


Figure 5. Dosage of $\text{Al}_{13}\text{-O-MMt}$ used in the adsorption of 30 mL 200 mg/L phosphorus solution with pH = 8, related to adsorption efficiency.

3.3. Column Adsorption of Phosphorus by $\text{Al}_{13}\text{-O-MMt}$ in the Elution Column and Breakthrough Time Analysis

In Figure 6, the adsorption efficiency dropped rapidly after day 10 in the column experiment. The adsorption efficiency was about 85%, which was lower than the efficiency of batch adsorption, implying that the adsorption approached saturation within 10 days. The calculation reveals that the phosphorus adsorption capacity of $\text{Al}_{13}\text{-O-MMt}$ in column adsorption is 60 mg/g, which is higher compared to that of other montmorillonite-based sorbents (Table 1).

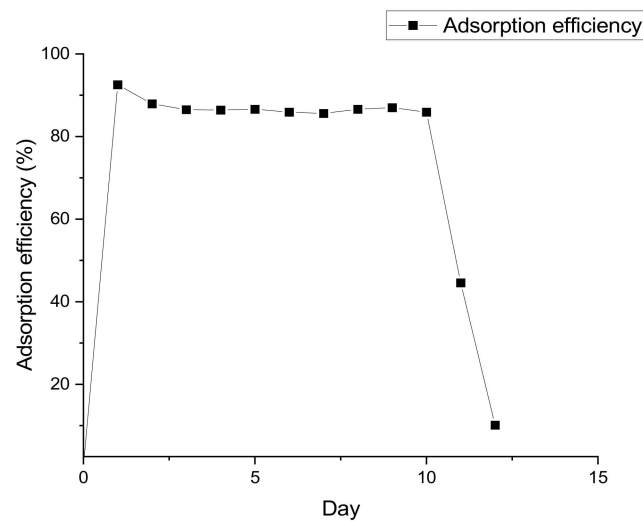


Figure 6. Column adsorption for 12 days (8 h/day) with a total of 2400 mL phosphorus solution (200 mg/L) with pH = 8.

Table 1. Comparison of phosphorus adsorption capacity and sorption condition among various montmorillonite-based adsorbents.

Sorbent	Experiment Condition			Sorption Capacity (mg/g)	Reference
	Adsorbent Dosage (g)	pH	Phosphorus Concentration (mg/L)		
Chitosan/Ca-organically modified montmorillonite beads	10	7	50	48.35	[16]
Fe-loaded ceramic adsorbent (contain montmorillonite)	10	6	10	45.88	[61]
Zirconium (Zr)-modified calcium-montmorillonite (Zr-CaMs)	2.5	4	50	22.37	[62]
Keggin Al ₁₃ complex-HDTMA-modified montmorillonite (Al ₁₃ -O-MMt)	6.667	8	200	60	This study

To verify the adsorption capacity of Al₁₃-O-MMt in the column experiment as to whether it met the expectation, the breakthrough time was calculated via Equation (2).

In Equation (2), the Thomas rate constant (k_{TH}) can be calculated using Equation (3):

$$k_{TH} = \frac{v}{m} \quad (3)$$

where v denotes the flow rate, and m represents the mass of phosphorus flowing in 1 min. Therefore,

$$k_{TH} = \frac{0.417 \text{ mL} \cdot \text{min}^{-1}}{200 \text{ mg} \cdot \text{L}^{-1} \times (0.417 \times 10^{-3}) \text{ L}} = 5 \text{ mL} \cdot \text{min}^{-1} \cdot \text{mg}^{-1}$$

If the values of the initial and equilibrium concentrations of solute in solution (c_0 and c), the adsorption capacity (q_0), the quantity of the montmorillonite used (x), the flow

rate (v), and the Thomas rate constant (k_{TH}) are known, the breakthrough time (t) can be calculated based on Equation (2). The transformations of Equation (2) are expressed as:

$$\begin{aligned}\frac{c}{c_0} &= \frac{1}{1 + \exp\left(\frac{k_{TH}q_0x}{v} - k_{TH}C_0t\right)} \\ \exp\left(\frac{k_{TH}q_0x}{v} - k_{TH}C_0t\right) &= \frac{c_0}{c} - 1 \\ \frac{k_{TH}q_0x}{v} - k_{TH}C_0t &= \ln\left(\frac{c_0}{c} - 1\right) \\ t &= \frac{\frac{k_{TH}q_0x}{v} - \ln\left(\frac{c_0}{c} - 1\right)}{k_{TH}C_0}\end{aligned}$$

Thus, the breakthrough time (t) can be calculated:

$$t = \frac{\frac{5 \text{ mL}\cdot\text{min}^{-1}\cdot\text{mg}^{-1}\times 60 \text{ mg}\cdot\text{g}^{-1}\times 6.667 \text{ g}}{0.417 \text{ mL}\cdot\text{min}^{-1}} - \ln\left(\frac{0.2 \text{ mg}\cdot\text{mL}^{-1}}{0.03 \text{ mg}\cdot\text{mL}^{-1}} - 1\right)}{5 \text{ mL}\cdot\text{min}^{-1}\cdot\text{mg}^{-1} \times 0.2 \text{ mg}\cdot\text{mL}^{-1}}$$

$$t = 4794.67 \text{ min}$$

After the calculation, the breakthrough time was 4794.67 min in the column experiment. This result indicates that when a phosphorus ion reached the bottom of the elution column, it took 4794.67 min to flow away in solution if it could pass the hurdle of being adsorbed by Al₁₃-O-MMt. This result also verifies that the predicted result of the batch experiment as applied to the column experiment is correct which means the Al₁₃-O-MMt in the column experiment met the expected adsorption capacity. Mesfer et al. demonstrated that a longer breakthrough time could indicate better adsorption efficiency and capacity [63]. Therefore, adsorption efficiency can be increased if the flow rate of the constant flow pump is reduced and the breakthrough time is increased. Nevertheless, this increase in breakthrough time to adsorption efficiency is not linear. Hence, an optimal operating efficiency should be guaranteed by reducing the flow rate to obtain a more reasonable phosphorus concentration in the solution, should this treatment be applied to industry.

3.4. Further Confirmation of Batch and Column Adsorptions of Phosphorus by XRD Analysis

In the batch and column adsorption experiment, chemical analysis confirmed that Al₁₃-O-MMt has a good ability to remove phosphorus in aqueous solution. To further determine the increase in the adsorption of phosphorus onto Al₁₃-O-MMt, the structural characteristics of Al₁₃-O-MMt before and after the adsorption of phosphorus were determined using XRD to verify whether alteration of the interlayer was related to such an increase in adsorption of phosphorus. According to Figure 7, the d_{001} peak was shifted to lower angles after modification, indicating that the interlayer distance within the layers of MMt increased. The increase in interlayer distance in Al₁₃-O-MMt was due to the intercalation of Keggin Al₁₃ complexes and HDTMA. The increase in interlayer distance could provide more sites for adsorbing phosphorus. After batch and column adsorptions, the d_{001} peak of Al₁₃-O-MMt was shifted to higher angles, suggesting a decrease in the interlayer distance of Al₁₃-O-MMt. This decrease in the interlayer distance of Al₁₃-O-MMt revealed that the phosphorus ions adsorbed by the Keggin Al₁₃ complex influenced the arrangement of modifiers in the interlayer [64]. Furthermore, the changed interlayer distance of modified MMt revealed that the increase in phosphorus adsorption was due to the increased interlayer, where the adsorption took place. Compared to the d_{001} peak of Al₁₃-O-MMt before and after batch adsorption, the d_{001} peak after column adsorption became much broader. This could be explained as follows: the aqueous phosphorus ions retained by Al₁₃-O-MMt in the column had a longer time to react with Keggin Al₁₃ complexes and HDTMA in the interlayer of Al₁₃-O-MMt, resulting in the disordered arrangement of modifiers in the interlayer—this reflected by the broader d_{001} peak as shown in Figure 7.

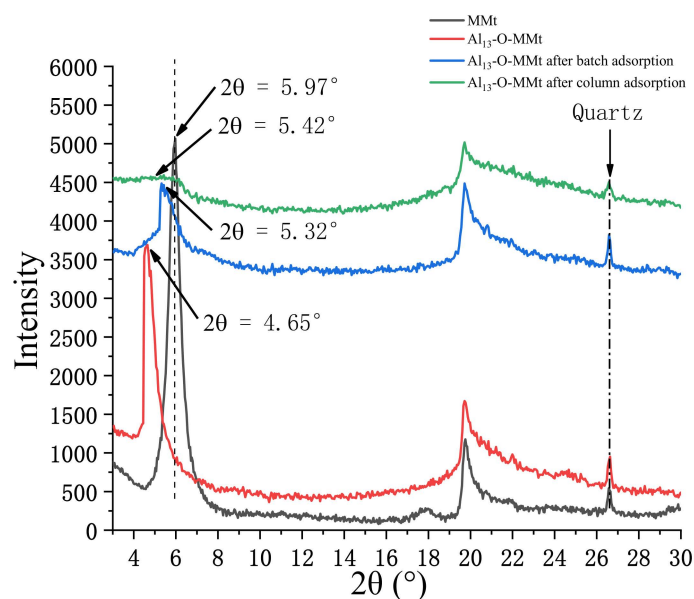


Figure 7. XRD pattern for comparison of MMT, Al₁₃-O-MMt, and Al₁₃-O-MMt after batch and column adsorption. 26.58° 2θ is the quartz diffraction used as the internal standard for spacing identification.

4. Conclusions

This research shows that montmorillonite modified by Keggin Al₁₃ complexes and HDTMA can more effectively remove phosphorus than MMT in aqueous solution. The high adsorption efficiency of phosphorus onto Al₁₃-O-MMt was due to the larger inter-layer distance and greater number of adsorption sites for phosphorus provided by the modifiers, Keggin Al₁₃ complex and HDTMA. The adsorption efficiency increased as the pH increased to 8, which implied the better adsorption of phosphorus in PO₄²⁻ form, which was transformed from HPO₄⁻ with increasing pH. The decrease in the adsorption efficiency with the further increase in pH to 9 was due to the increase in the negative charge on the surface, resulting in more electrostatic repulsion between the adsorbent and phosphorus. Since the phosphorus adsorption process by Al₁₃-O-MMt is spontaneously exothermic, the adsorption ability of Al₁₃-O-MMt decreased with increasing temperature. The breakthrough time was 4794.67 min, verifying that the adsorption of phosphorus onto Al₁₃-O-MMt in the column experiment met the expected adsorption capacity in the batch experiment.

Author Contributions: The conceptualization was by J.C. and H.D.R.; methodology, J.C. and H.D.R.; validation, H.D.R.; formal analysis, Z.H.; data curation, Z.H.; writing—original draft preparation, Z.H.; writing—review and editing, J.C., J.L., L.S., S.Y.J., C.H.L. and H.D.R.; supervision, H.D.R.; project administration, H.D.R.; and funding acquisition by H.D.R. and S.Y.J. All authors have read and agreed to the published version of the manuscript.

Funding: This work is supported in part by Guangdong Department of Education (2020-2023) of the “Research Platform and Research Project” No. 2020ZDZX1022, and UIC Research Grant No. UICR5202018 at BNU-HKBU United International College, Zhuhai, PR China; Guangdong High Education Youth Creation Grant No. 2020KQNCX099, and UIC Research Grant No. UICR5202016 at BNU-HKBU United International College, Zhuhai, PR China; and UIC Research Grants Nos. R202011, R25202016, R5202018, and R201805 at BNU-HKBU United International College, Zhuhai, PR China.

Institutional Review Board Statement: Not applicable.

Informed Consent Statement: Not applicable.

Data Availability Statement: Not applicable.

Acknowledgments: The authors thank Wang Mingchong, Li Tao, and Wang Sijian, who provided comments for this work.

Conflicts of Interest: The authors declare no conflict of interest. The funders had no role in the design of the study; in the collection, analysis, or interpretation of data; in the writing of the manuscript; or in the decision to publish the results.

References

1. Gutiérrez, G.G. *Oxydation of Clay Nanoreinforced Polyolefins*; Arts et Métiers ParisTech: Paris, France, 2010.
2. Uddin, F. *Montmorillonite: An Introduction to Properties and Utilization*; IntechOpen: London, UK, 2018.
3. Shao, Y.; Gan, Z.; Epifanovsky, E.; Gilbert, A.T.; Wormit, M.; Kussmann, J.; Lange, A.W.; Behn, A.; Deng, J.; Feng, X. Advances in molecular quantum chemistry contained in the Q-Chem 4 program package. *Mol. Phys.* **2015**, *113*, 184–215. [[CrossRef](#)]
4. Ahmed, A.; Chaker, Y.; Belarbi, E.H.; Abbas, O.; Chotard, J.; Abassi, H.; Van Nhien, A.N.; El Hadri, M.; Bresson, S. XRD and ATR/FTIR investigations of various montmorillonite clays modified by monocationic and dicationic imidazolium ionic liquids. *J. Mol. Struct.* **2018**, *1173*, 653–664. [[CrossRef](#)]
5. Gu, S.; Kang, X.; Wang, L.; Lichtfouse, E.; Wang, C. Clay mineral adsorbents for heavy metal removal from wastewater: A review. *Environ. Chem. Lett.* **2019**, *17*, 629–654. [[CrossRef](#)]
6. Wang, J.; Xu, Y.; Han, Y.; Yan, L.; Wei, Q. Study on Adsorption Properties of modified montmorillonite for organic pollutants. *J. Univ. Jinan* **2008**, *1*, 72–76. [[CrossRef](#)]
7. Li, Y.; Narayanan Nair, A.K.; Kadoura, A.; Yang, Y.; Sun, S. Molecular simulation study of montmorillonite in contact with water. *Ind. Eng. Chem. Res.* **2019**, *58*, 1396–1403. [[CrossRef](#)]
8. Ilari, R.; Etcheverry, M.; Waiman, C.V.; Zanini, G.P. A simple cation exchange model to assess the competitive adsorption between the herbicide paraquat and the biocide benzalkonium chloride on montmorillonite. *Colloids Surf. A Physicochem. Eng. Asp.* **2021**, *611*, 125797. [[CrossRef](#)]
9. Zeng, G.; Liu, Y.; Tang, L.; Yang, G.; Pang, Y.; Zhang, Y. Enhancement of Cd(II) adsorption by polyacrylic acid modified magnetic mesoporous carbon. *Chem. Eng. J.* **2015**, *259*, 153–160. [[CrossRef](#)]
10. Jinxu, N.; Wenguang, T.; Mi, L.; Pengjun, Y. Research on preparation of modified bentonite and its removal of ammonia nitrogen and phosphorus from Wastewater. In Proceedings of the 2011 International Conference on Electric Technology and Civil Engineering (ICETCE), Lushan, China, 22–24 April 2011; pp. 6799–6804.
11. Kalaiselvi, J.; Selvakumar, K.; Rajendran, S.; Sowmya, G.; Ramesh Prabhu, M. Effect of surface-modified montmorillonite incorporated biopolymer membranes for PEM fuel cell applications. *Polym. Compos.* **2019**, *40*, E301–E311. [[CrossRef](#)]
12. Hu, X.; Ke, Y. The influence of organic modified montmorillonite on the solution properties of copolymer containing β -cyclodextrin. *J. Polym. Res.* **2020**, *27*, 19. [[CrossRef](#)]
13. Xiao, F.; Yan, B.-Q.; Zou, X.-Y.; Cao, X.-Q.; Dong, L.; Lyu, X.-J.; Li, L.; Qiu, J.; Chen, P.; Hu, S.-G. Study on ionic liquid modified montmorillonite and molecular dynamics simulation. *Colloids Surf. A Physicochem. Eng. Asp.* **2020**, *587*, 124311. [[CrossRef](#)]
14. Liu, S.; Chen, M.; Cao, X.; Li, G.; Zhang, D.; Li, M.; Meng, N.; Yin, J.; Yan, B. Chromium (VI) removal from water using cetylpyridinium chloride (CPC)-modified montmorillonite. *Sep. Purif. Technol.* **2020**, *241*, 116732. [[CrossRef](#)]
15. Abdel-Karim, A.; El-Naggar, M.E.; Radwan, E.; Mohamed, I.M.; Azaam, M.; Kenawy, E.-R. High-performance mixed-matrix membranes enabled by organically/inorganic modified montmorillonite for the treatment of hazardous textile wastewater. *Chem. Eng. J.* **2021**, *405*, 126964. [[CrossRef](#)]
16. Jang, J.; Lee, D.S. Effective phosphorus removal using chitosan/Ca-organically modified montmorillonite beads in batch and fixed-bed column studies. *J. Hazard. Mater.* **2019**, *375*, 9–18. [[CrossRef](#)] [[PubMed](#)]
17. Ong, L.; Soetaredjo, F.; Kurniawan, A.; Ayucitra, A.; Liu, J.-C.; Ismadji, S. Investigation on the montmorillonite adsorption of biocidal compounds incorporating thermodynamical-based multicomponent adsorption isotherm. *Chem. Eng. J.* **2014**, *241*, 9–18. [[CrossRef](#)]
18. Yi, H.; Jia, F.; Zhao, Y.; Wang, W.; Song, S.; Li, H.; Liu, C. Surface wettability of montmorillonite (0 0 1) surface as affected by surface charge and exchangeable cations: A molecular dynamic study. *Appl. Surf. Sci.* **2018**, *459*, 148–154. [[CrossRef](#)]
19. Del Mar Orta, M.; Martín, J.; Medina-Carrasco, S.; Santos, J.L.; Aparicio, I.; Alonso, E. Adsorption of propranolol onto montmorillonite: Kinetic, isotherm and pH studies. *Appl. Clay Sci.* **2019**, *173*, 107–114. [[CrossRef](#)]
20. Camacho, L.M.; Deng, S.; Parra, R.R. Uranium removal from groundwater by natural clinoptilolite zeolite: Effects of pH and initial feed concentration. *J. Hazard. Mater.* **2010**, *175*, 393–398. [[CrossRef](#)]
21. Almasri, D.A.; Rhadfi, T.; Atieh, M.A.; McKay, G.; Ahzi, S. High performance hydroxyiron modified montmorillonite nanoclay adsorbent for arsenite removal. *Chem. Eng. J.* **2018**, *335*, 1–12. [[CrossRef](#)]
22. Wang, Y.-Q.; Zheng, Z.-Y.; Zhao, Y.-K.; Huang, J.-H.; Zhang, Z.-B.; Cao, X.-H.; Dai, Y.; Hua, R.; Liu, Y.-H. Adsorption of U (VI) on montmorillonite pillared with hydroxy-aluminum. *J. Radioanal. Nucl. Chem.* **2018**, *317*, 69–80. [[CrossRef](#)]
23. Rezala, H.; Douba, H.; Boukhatem, H.; Romero, A. Adsorption of methylene blue by hydroxyl-aluminum pillared montmorillonite. *J. Chem. Soc. Pak.* **2020**, *42*, 550–563.
24. Ruiz, G. Effect of salinity and temperature on the adsorption of Hg(II) from aqueous solutions by a Ca-montmorillonite. *Environ. Technol.* **2009**, *30*, 63–68. [[CrossRef](#)] [[PubMed](#)]
25. Ma, J.; Lei, Y.; Khan, M.A.; Wang, F.; Chu, Y.; Lei, W.; Xia, M.; Zhu, S. Adsorption properties, kinetics & thermodynamics of tetracycline on carboxymethyl-chitosan reformed montmorillonite. *Int. J. Biol. Macromol.* **2019**, *124*, 557–567. [[PubMed](#)]

26. Wu, K.; Ye, Q.; Wu, R.; Dai, H. Alkali metal-promoted aluminum-pillared montmorillonites: High-performance CO₂ adsorbents. *J. Solid State Chem.* **2020**, *291*, 121585. [[CrossRef](#)]
27. Chauhan, M.; Saini, V.K.; Suthar, S. Removal of pharmaceuticals and personal care products (PPCPs) from water by adsorption on aluminum pillared clay. *J. Porous Mater.* **2020**, *27*, 383–393. [[CrossRef](#)]
28. Zou, X.-Y.; Xiao, F.; Liu, S.-R.; Cao, X.-Q.; Li, L.; Chen, M.; Dong, L.; Lyu, X.-J.; Gai, Y.-J. Preparation and application of CPC/Keggin-Al₃₀ modified montmorillonite composite for Cr (VI) removal. *J. Water Process Eng.* **2020**, *37*, 101348. [[CrossRef](#)]
29. Wang, M.; Orr, A.A.; He, S.; Dalaijants, C.; Chiu, W.A.; Tamamis, P.; Phillips, T.D. Montmorillonites can tightly bind glyphosate and paraquat reducing toxin exposures and toxicity. *ACS Omega* **2019**, *4*, 17702–17713. [[CrossRef](#)]
30. Manohar, D.M.; Krishnan, K.A.; Anirudhan, T.S. Removal of mercury(II) from aqueous solutions and chlor-alkali industry wastewater using 2-mercaptobenzimidazole-clay. *Water Res.* **2002**, *36*, 1609–1619. [[CrossRef](#)]
31. Umpuch, C.; Sopasin, S. Adsorption of Malachite Green by Chitosan Modified Montmorillonite. In Proceedings of the International Science and Technology Conference, Paris, France, 18–20 July 2018; p. 53.
32. França, D.; Oliveira, L.; Nunes Filho, F.; Silva Filho, E.; Osajima, J.; Jaber, M.; Fonseca, M. The Versatility of Montmorillonite in Water Remediation Using Adsorption: Current Studies and Challenges in Drug Removal. *J. Environ. Chem. Eng.* **2022**, *10*, 107341. [[CrossRef](#)]
33. Wibulswas, R. Batch and fixed bed sorption of methylene blue on precursor and QACs modified montmorillonite. *Sep. Purif. Technol.* **2004**, *39*, 3–12. [[CrossRef](#)]
34. Zelaya Soulé, M.E.; Flores, F.M.; Torres Sánchez, R.M.; Fernández, M.A. Norfloxacin adsorption on montmorillonite and carbon/montmorillonite hybrids: pH effects on the adsorption mechanism, and column assays. *J. Environ. Sci. Health Part A* **2020**, *56*, 113–122. [[CrossRef](#)]
35. Yotsuji, K.; Tachi, Y.; Sakuma, H.; Kawamura, K. Effect of interlayer cations on montmorillonite swelling: Comparison between molecular dynamic simulations and experiments. *Appl. Clay Sci.* **2021**, *204*, 106034. [[CrossRef](#)]
36. Peng, J.; Yi, H.; Song, S.; Zhan, W.; Zhao, Y. Driving force for the swelling of montmorillonite as affected by surface charge and exchangeable cations: A molecular dynamic study. *Results Phys.* **2019**, *12*, 113–117. [[CrossRef](#)]
37. Yang, J.; Wang, S.; Xu, N.; Ye, Z.; Yang, H.; Huangfu, X. Synthesis of montmorillonite-supported nano-zero-valent iron via green tea extract: Enhanced transport and application for hexavalent chromium removal from water and soil. *J. Hazard. Mater.* **2021**, *419*, 126461. [[CrossRef](#)] [[PubMed](#)]
38. Daño, M.; Viglašová, E.; Galamboš, M.; Štamberg, K.; Kujan, J. Surface complexation models of pertechnetate on biochar/montmorillonite composite—Batch and dynamic sorption study. *Materials* **2020**, *13*, 3108. [[CrossRef](#)]
39. Lawal, I.A.; Moodley, B. Fixed-bed and batch Adsorption of pharmaceuticals from aqueous solutions on ionic liquid-modified montmorillonite. *Chem. Eng. Technol.* **2018**, *41*, 983–993. [[CrossRef](#)]
40. Deng, L.; Liu, Y.; Zhuang, G.; Yuan, P.; Liu, D.; Bu, H.; Song, H.; Li, L. Dynamic benzene adsorption performance of microporous TMA⁺-exchanged montmorillonite: The role of TMA⁺ cations. *Microporous Mesoporous Mater.* **2020**, *296*, 109994. [[CrossRef](#)]
41. Guo, P.; Xu, N.; Li, D.; Huangfu, X.; Li, Z. Aggregation and transport of rutile titanium dioxide nanoparticles with montmorillonite and diatomite in the presence of phosphate in porous sand. *Chemosphere* **2018**, *204*, 327–334. [[CrossRef](#)]
42. Tong, Y.; Wang, M.; Peñuelas, J.; Liu, X.; Paerl, H.W.; Elser, J.J.; Sardans, J.; Couture, R.-M.; Larssen, T.; Hu, H. Improvement in municipal wastewater treatment alters lake nitrogen to phosphorus ratios in populated regions. *Proc. Natl. Acad. Sci. USA* **2020**, *117*, 11566–11572. [[CrossRef](#)]
43. Zhang, Q.; Yang, W.; Ngo, H.; Guo, W.; Jin, P.; Dzakpasu, M.; Yang, S.; Wang, Q.; Wang, X.; Ao, D. Current status of urban wastewater treatment plants in China. *Environ. Int.* **2016**, *92*, 11–22. [[CrossRef](#)]
44. Shi, J.; Xu, C.; Han, Y.; Han, H. Case study on wastewater treatment technology of coal chemical industry in China. *Crit. Rev. Environ. Sci. Technol.* **2021**, *51*, 1003–1044. [[CrossRef](#)]
45. Liang, H.; Liu, J.; Wei, Y.; Guo, X. Evaluation of phosphorus removal from wastewater by soils in rural areas in China. *J. Environ. Sci.* **2010**, *22*, 15–22. [[CrossRef](#)]
46. *Indicators: Phosphorus*; Environmental Protection Agency: Washington, DC, USA, 2021.
47. Nieder, R.; Benbi, D.K.; Reichl, F.X. Reactive water-soluble forms of nitrogen and phosphorus and their impacts on environment and human health. In *Soil Components and Human Health*; Springer: Dordrecht, The Netherlands, 2018; pp. 223–255.
48. D’Haese, P.C.; Douglas, G.; Verhulst, A.; Neven, E.; Behets, G.J.; Vervaeke, B.A.; Finsterle, K.; Lürling, M.; Spears, B. Human health risk associated with the management of phosphorus in freshwaters using lanthanum and aluminium. *Chemosphere* **2019**, *220*, 286–299. [[CrossRef](#)] [[PubMed](#)]
49. Ruan, H.D.; Gilkes, R.J. Accumulation of phosphorus in farm ponds and dams in South-Western Australia. *J. Environ. Qual.* **2000**, *29*, 1875–1881. [[CrossRef](#)]
50. Elsheikh, M.A.; Muchaonyerwa, P.; Johan, E.; Matsue, N.; Henmi, T. Mutual adsorption of lead and phosphorus onto selected soil clay minerals. *Adv. Chem. Eng. Sci.* **2018**, *8*, 67–81. [[CrossRef](#)]
51. McTaggart, W.S. Characterization of Acid Phosphatase Adsorption to Montmorillonite. *FASEB J.* **2018**, *32*, 533.75. [[CrossRef](#)]
52. Soulé, M.Z.; Fernández, M.; Montes, M.L.; Suárez-García, F.; Sánchez, R.T.; Tascón, J. Montmorillonite-hydrothermal carbon nanocomposites: Synthesis, characterization and evaluation of pesticides retention for potential treatment of agricultural wastewater. *Colloids Surf. A Physicochem. Eng. Asp.* **2020**, *586*, 124192. [[CrossRef](#)]

53. Ma, L.; Zhu, J.; Xi, Y.; Zhu, R.; He, H.; Liang, X.; Ayoko, G.A. Adsorption of phenol, phosphate and Cd (II) by inorganic–organic montmorillonites: A comparative study of single and multiple solute. *Colloids Surf. A Physicochem. Eng. Asp.* **2016**, *497*, 63–71. [[CrossRef](#)]
54. Sahir, A.H.; Kumar, S.; Kumar, S. Modelling of a packed bed solid-state fermentation bioreactor using the N-tanks in series approach. *Biochem. Eng. J.* **2007**, *35*, 20–28. [[CrossRef](#)]
55. Mnasri, S.; Frini-Srasra, N. Evolution of Brønsted and Lewis acidity of single and mixed pillared bentonite. *Infrared Phys. Technol.* **2013**, *58*, 15–20. [[CrossRef](#)]
56. Chen, J.; Lu, J.; Su, L.; Ruan, H.; Zhao, Y.; Lee, C.; Cai, Z.; Wu, Z.; Jiang, Y. Enhanced Adsorption of Methyl Orange by Mongolian Montmorillonite after Aluminum Pillaring. *Appl. Sci.* **2022**, *12*, 3182. [[CrossRef](#)]
57. Ge, Z.; Li, D.; Pinnavaia, T.J. Preparation of alumina-pillared montmorillonites with high thermal stability, regular microporosity and Lewis/Brønsted acidity. *Microporous Mater.* **1994**, *3*, 165–175. [[CrossRef](#)]
58. Lin, J.; He, S.; Zhan, Y.; Zhang, Z.; Wu, X.; Yu, Y.; Zhao, Y.; Wang, Y. Assessment of sediment capping with zirconium-modified bentonite to intercept phosphorus release from sediments. *Environ. Sci. Pollut. Res.* **2019**, *26*, 3501–3516. [[CrossRef](#)] [[PubMed](#)]
59. Zhang, H.; Zhao, F.; Xia, M.; Wang, F. Microscopic adsorption mechanism of montmorillonite for common ciprofloxacin emerging contaminant: Molecular dynamics simulation and Multiwfn wave function analysis. *Colloids Surf. A Physicochem. Eng. Asp.* **2021**, *614*, 126186. [[CrossRef](#)]
60. Akram, M.; Bhatti, H.N.; Iqbal, M.; Noreen, S.; Sadaf, S. Biocomposite efficiency for Cr (VI) adsorption: Kinetic, equilibrium and thermodynamics studies. *J. Environ. Chem. Eng.* **2017**, *5*, 400–411. [[CrossRef](#)]
61. Wang, D.; Chen, N.; Yu, Y.; Hu, W.; Feng, C. Investigation on the adsorption of phosphorus by Fe-loaded ceramic adsorbent. *J. Colloid Interface Sci.* **2016**, *464*, 277–284. [[CrossRef](#)]
62. Zou, Y.; Zhang, R.; Wang, L.; Xue, K.; Chen, J. Strong adsorption of phosphate from aqueous solution by zirconium-loaded Ca-montmorillonite. *Appl. Clay Sci.* **2020**, *192*, 105638. [[CrossRef](#)]
63. Al Mesfer, M.K.; Danish, M. Breakthrough adsorption study of activated carbons for CO₂ separation from flue gas. *J. Environ. Chem. Eng.* **2018**, *6*, 4514–4524. [[CrossRef](#)]
64. Garaga, M.N. Locale Structure around Heteroatoms in Alumino-and Borosilicates for Catalysis. Ph.D. Thesis, Université d’Orléans, Orléans, France, 2013.